Inorg. Chem. **2004**, *43*, 5645–5658

Pseudooctahedral Complexes of Vanadium(III): Electronic Structure Investigation by Magnetic and Electronic Spectroscopy

J. Krzystek,[†] Adam T. Fiedler,[‡] Jennifer J. Sokol,[§] Andrew Ozarowski,[†] S. A. Zvyagin,[†] Thomas C. Brunold,[‡] Jeffrey R. Long,[§] Louis-Claude Brunel,[†] and Joshua Telser*,[||]

National High Magnetic Field Laboratory, Florida State University, Tallahassee, Florida 32310, Department of Chemistry, University of Wisconsin, Madison, Wisconsin 53706, Department of Chemistry, University of California, Berkeley, California 94720, and Chemistry Program, Roosevelt University, Chicago, Illinois 60605

Received May 18, 2004

A variety of physical methods has been used to probe the non-Kramers, $S = 1$, V(III) ion in two types of pseudooctahedral complexes: $V(acac)_3$, where acac = anion of 2,4-pentanedione, and $VX_3(thf)_3$, where thf = tetrahydrofuran and X = Cl and Br. These methods include tunable frequency and high-field electron paramagnetic resonance (HFEPR) spectroscopy (using frequencies of ~95–700 GHz and fields up to 25 T) in conjunction with electronic absorption, magnetic circular dichroism (MCD), and variable-temperature variable-field MCD (VTVH-MCD) spectroscopies. Variable-temperature magnetic susceptibility and field-dependent magnetization measurements were also performed. All measurements were conducted on complexes in the solid state (powder or mull samples). The field versus sub-THz wave quantum energy dependence of observed HFEPR resonances yielded the following spin Hamiltonian parameters for $V(acac)_3$: $D = +7.470(1)$ cm^{-1}; $E = +1.916(1)$ cm^{-1}; $g_x = 1.833(4)$; $g_y = 1.72(2)$; $g_z = 2.03(2)$. For $VCl_3(thf)_3$, HFEPR detected a single zero-field transition at 15.8 cm^{-1} (474 GHz), which was insufficient to determine the complete set of spin Hamiltonian parameters. For $VBr_3(thf)_3$, however, a particularly rich data set was obtained using tunable-frequency HFEPR, and analysis of this data set gave the folowing: $D = -16.162(6)$ cm^{-1}; $E = -3.694(4)$ cm^{-1}; $g_x = 1.86(1)$; $g_y = 1.90(1)$; $g_z = 1.710(4)$. Analysis of the VTVH-MCD data gave spin Hamiltonian parameters in good agreement with those determined by HFEPR for both $V(acac)_3$ and $VBr_3(thf)_3$ and in rough agreement with the estimate for $VCl_3(thf)_3$ ($D \approx 10$ cm^{-1}, $|E/D| \approx 0.18$), together with the finding that the value of D is negative for both thf complexes. The electronic structures of these V(III) complexes are discussed in terms of their molecular structures and the electronic transitions observed by electronic absorption and MCD spectroscopies.

Introduction

Vanadium(III) ($3d^2$, $S = 1$) is of inherent interest as a relatively less explored oxidation state of vanadium with relevance to the bioinorganic chemistry of marine organisms.[1] V(III) complexes have also found applications as insulin-enhancing agents.[2] Of particular significance to us is the recent use of V(III) complexes as building blocks for single-molecule magnets[3] and the synthesis of novel layered materials that contain V(III).[4−6] A better understanding of the electronic structure of such multinuclear V(III) systems will result from detailed studies on mononuclear V(III) complexes.

Indeed, V(III) was the subject of a number of pioneering studies involving both optical[7] and magnetic resonance

* Author to whom correspondence should be addressed. E-mail: jtelser@roosevelt.edu.
[†] Florida State University.
[‡] University of Wisconsin.
[§] University of California.
[||] Roosevelt University.

(1) Butler, A.; Carrano, C. J. *Coord. Chem. Rev.* **1991**, *109*, 61−105.
(2) Melchior, M.; Rettig, S. J.; Liboiron, B. D.; Thompson, K. H.; Yuen, V. G.; McNeill, J. H.; Orvig, C. *Inorg. Chem.* **2001**, *40*, 4686−4690.
(3) Castro, S. L.; Sun, Z.; Grant, C. M.; Bollinger, J. C.; Hendrickson, D. N.; Christou, G. *J. Am. Chem. Soc.* **1998**, *120*, 2365−2375.
(4) Grohol, D.; Nocera, D. G. *J. Am. Chem. Soc.* **2002**, *124*, 2640−2646.
(5) Papoutsakis, D.; Grohol, D.; Nocera, D. G. *J. Am. Chem. Soc.* **2002**, *124*, 2647−2656.
(6) Grohol, D.; Papoutsakis, D.; Nocera, D. G. *Angew. Chem., Int. Ed.* **2001**, *40*, 1519−1521.
(7) Pryce, M. H. L.; Runciman, W. A. *Discuss. Faraday Soc.* **1958**, *26*, 34−42.

10.1021/ic0493503 CCC: $27.50
Published on Web 08/04/2004

spectroscopy.[8−11] The EPR[12] studies are of particular note since transition metal systems with $S = 1$ and lower than cubic symmetry are often "EPR silent" using conventional spectrometers. This "silence" is the result of the zero-field splitting (zfs, with the axial component represented by D and the rhombic component by E) being much larger than the microwave quantum ($\sim$0.3 cm^{-1} for X-band EPR), such that no spin-allowed ($\Delta M_S = \pm 1$) EPR transitions are within the frequency/field range. When the symmetry about the metal ion is high, the zfs is small and such systems are then amenable to conventional EPR. For instance, a V(III) tetraalkyl complex with a slightly distorted tetrahedral symmetry and $D = 0.45$ cm^{-1} was observable by X-band EPR.[13]

In certain cases, however, it is possible to observe nominally forbidden ($|\Delta M_S| > 1$) EPR transitions in EPR silent systems. Zverev and Prokhorov observed a $\Delta M_S = \pm 2$ ($M_S = \pm 1 \leftrightarrow \mp 1$) signal at frequencies up to ca. 38 GHz for V(III) as a dopant in corundum (Al_2O_3) and noted that "the detection of $|\Delta M| = 1$ lines would be of considerable interest but would require the construction of a microwave spectrometer for the 150−250 [GHz] range".[8] Remarkably, this was achieved by Sauzade et al. a few years later, who detected $\Delta M_S = \pm 1$ transitions in the same material at 144.55 GHz.[14] Foner and Low had, in fact, already observed $\Delta M_S = \pm 1$ transitions in this material by the use of moderately high frequencies (36 and 71 GHz) but with very high magnetic fields (up to 50 T) obtained with a pulsed magnet.[9] Shortly thereafter, Joyce and Richards used a far-infrared spectrometer (operating range 2−300 cm^{-1}, with fixed magnetic fields up to 5.5 T) to observe all of the relevant magnetic resonance transitions for V(III) in Al_2O_3.[15] Despite these early successes, magnetic resonance studies of $S = 1$ transition metal ion systems were pursued little further. The advent of high-frequency and -field EPR (HFEPR; $\nu > 94$ GHz; B_0 up to $\sim$25 T) spectrometers has led to a resurgence of interest in high-spin systems in general,[16] with applications to materials science[17,18] and bioinorganic chemistry in particular.[19]

Accordingly, modern HFEPR spectroscopy has been recently applied to V(III) and its "hole" counterpart, Ni(II) ($3d^8$). In the case of Ni(II), HFEPR studies have been performed on the paramagnetic ion doped into diamagnetic hosts[20,21] and on pure molecular complexes.[22,23] Concerning V(III), very beautiful HFEPR studies were recently reported for V(III) as the sole 3+ ion in a RbV alum[24] and as a dopant in a CsGa alum,[25] where MM′ alum represents the following class of salts: $(M^+)(M'^{3+})([S,Se,Te]O_4)_2 \cdot 12H_2O$. To our knowledge, however, no HFEPR studies have ever been made on complexes of V(III) with other than an O_6 donor set (oxo or aqua ligands). We have therefore performed studies on several molecular complexes in which V(III) is found in highly distorted pseudooctahedral environments, yielding $S = 1$ ground states with significant zfs. The specific systems investigated are of two chemical/structural types, as shown in Chart 1: $V(acac)_3$, where acac = anion of 2,4-pentanedione, and $VX_3(thf)_3$, where thf = tetrahydrofuran and X = Cl and Br (the corresponding complex with X = I has not been prepared). Crystal structures have been reported for $V(acac)_3$[26] and $VCl_3(thf)_3$[27] but not for $VBr_3(thf)_3$. $V(acac)_3$ crystallizes in two forms, α and β, which have slightly different structural parameters, although both show trigonal distortions about the V(III) ion.[26,28] The predilection for one or the other crystal forms is not known. $VCl_3(thf)_3$ (and presumably the Br complex) has meridional geometry (as do $MCl_3(thf)_3$, where M = Sc, Ti, Cr) and approximate C_{2v} symmetry about the V(III) ion.[27] The two types of complexes thus represent rather different forms of distorted octahedral geometries.

Chart 1

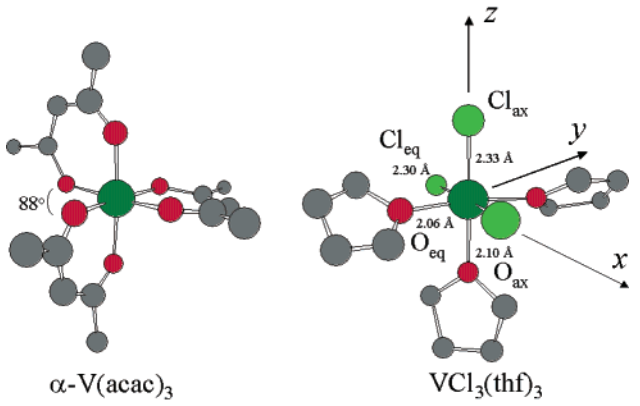

Equally important as the molecular structures are the corresponding electronic structures of the V(III) complexes

(8) Zverev, G. M.; Prokhorov, A. M. *Sov. Phys. JETP* **1960**, *11*, 330−333.
(9) Foner, S.; Low, W. *Phys. Rev.* **1960**, *120*, 1585−1588.
(10) Schwartz, R. W.; Carlin, R. L. *J. Am. Chem. Soc.* **1970**, *92*, 6763−6771.
(11) Clarke, J. G.; MacKinnon, J. A. *Can. J. Phys.* **1971**, *49*, 1539−1541.
(12) Abbreviations used: AOM, angular overlap model; BWO, backwards wave oscillator; CT, charge-transfer; EPR, electron paramagnetic resonance; HFEPR, high-frequency and -field EPR; LF, ligand field; S/N, signal-to-noise ratio; thf, tetrahydrofuran; zfs, zero-field splitting.
(13) Alonso, P. J.; Forniés, J.; García-Monforte, M. A.; Martín, A.; Menjón, B. *Chem. Commun.* **2001**, 2138−2139.
(14) Sauzade, M.; Pontnau, J.; Lesas, P.; Silhouette, D. *Phys. Lett.* **1966**, *19*, 617−618.
(15) Joyce, R. R.; Richards, P. L. *Phys. Rev.* **1969**, *179*, 375−380.
(16) Riedi, P. C.; Smith, G. M. In *Electron Paramagnetic Resonance*; Gilbert, B. C., Davies, M. J., Murphy, D. M., Eds.; Royal Society of Chemistry: Cambridge, U.K., 2002; Vol. 18, pp 254−303.
(17) Barra, A.-L.; Brunel, L.-C.; Gatteschi, D.; Pardi, L.; Sessoli, R. *Acc. Chem. Res.* **1998**, *31*, 460−466.
(18) Brunel, L.-C. *Physica B* **1995**, 360−362.
(19) Hagen, W. *Coord. Chem. Rev.* **1999**, *190*, 209−229.
(20) van Dam, P. J.; Klaassen, A. A. K.; Reijerse, E. J.; Hagen, W. R. *J. Magn. Reson.* **1998**, *130*, 140−144.
(21) Pardi, L. A.; Hassan, A. K.; Hulsbergen, F. B.; Reedijk, J.; Spek, A. L.; Brunel, L.-C. *Inorg. Chem.* **2000**, *39*, 159−164.
(22) Collison, D.; Helliwell, M.; Jones, V. M.; Mabbs, F. E.; McInnes, A. J. L.; Riedi, P. C.; Smith, G. M.; Pritchard, R. G.; Cross, W. I. *J. Chem. Soc., Faraday Trans.* **1998**, *94*, 3019−3025.
(23) Krzystek, J.; Park, J.-H.; Meisel, M. W.; Hitchman, M. A.; Stratemeier, H.; Brunel, L.-C.; Telser, J. *Inorg. Chem.* **2002**, *41*, 4478−4487.
(24) Tregenna-Piggott, P. L. W.; Best, S. P.; Güdel, H.-U.; Weihe, H.; Wilson, C. C. *J. Solid State Chem.* **1999**, *145*, 460−470.
(25) Tregenna-Piggott, P. L. W.; Weihe, H.; Bendix, J.; Barra, A.-L.; Güdel, H.-U. *Inorg. Chem.* **1999**, *38*, 5928−5929.
(26) Morosin, B.; Montgomery, H. *Acta Crystallogr.* **1969**, *B25*, 1354−1359.
(27) Cotton, F. A.; Duraj, S. A.; Powell, G. L.; Roth, W. J. *Inorg. Chim. Acta* **1986**, *113*, 81−85.
(28) The intra-ring O−V−O angles are 88.0° in the α form and 87.3° in the β form.

as determined by spectroscopy. Vanadium(III) hexa oxo/aqua species have been well studied by electronic absorption[7,24,29,30] and electronic Raman spectroscopy,[31] as well as by theory.[30,32] For the complexes studied herein, significantly less data are available. Piper and Carlin reported single-crystal electronic spectra for V(III) (as well as other for M^{3+} ions) doped into $Al(acac)_3$.[33] Machin and Murray reported diffuse reflectance electronic absorption spectra for both $V(acac)_3$ and $VCl_3(thf)_3$, although not for the Br complex.[34] As a result, we have investigated the three compounds of interest by electronic absorption, magnetic circular dichroism (MCD), and variable-temperature variable-field MCD (VTVH-MCD) spectroscopies. MCD has been widely applied to biologically relevant transition metal complexes and metalloproteins,[35,36] but to our knowledge it has never been used to study V(III) complexes. This technique provides insights into electronic transitions that are not available from electronic absorption spectroscopy, and analysis of the VTVH-MCD data yields information regarding the spin Hamiltonian parameters that is complementary to that obtained from HFEPR.[37]

Magnetic susceptibility studies of a wider variety of V(III) complexes have been reported over many years; most notable is the work of Figgis[38,39] and Carlin[40,41] as well as others.[34,42,43] Machin and Murray reported powder magnetic susceptibility data for $V(acac)_3$ and $VCl_3(thf)_3$ but over only the temperature range ~80−300 K.[34] A more recent magnetic study has also been reported for $V(acac)_3$, providing data for the range of 20−120 K.[42] For corroboration of these earlier magnetic studies with our current spectroscopic experiments, we have recorded powder magnetic susceptibility data over a wide temperature range for the three V(III) complexes of interest and performed field-dependent magnetization studies of the two thf complexes.

Experimental Section

Materials. Both $VCl_3(thf)_3$ and $VBr_3(thf)_3$ are commercially available (Aldrich); however, we did not find the purity of either of these materials to be satisfactory for HFEPR, MCD, or magnetic measurements. Commercial $VCl_3(thf)_3$, as received by us, was orange in color, which suggests the presence of $VCl_3(thf)_{3-n}(H_2O)_n$ ($n = 1$ and/or possibly 2), by comparison with a report of authentic $VCl_3(thf)_2(H_2O)$.[44] IR spectra of commercial $VCl_3(thf)_3$ did contain an absorption band at ca. 3300 cm^{-1}, assignable to ν(OH). Therefore, following literature procedures,[45] we synthesized $VX_3(thf)_3$ from commercial (Aldrich) VX_3 (X = Cl, Br) and thf, freshly distilled under nitrogen from sodium benzophenone ketyl. $VCl_3(thf)_3$ and $VBr_3(thf)_3$ prepared in this manner and maintained under rigorously air- and moisture-free atmosphere are respectively salmon pink and dark orange in color, as originally reported.[46] Authentic $VX_3(thf)_3$ is extremely hygroscopic and decomposes even under nitrogen, over a prolonged period, to yield initially orange (for X = Cl) and dark brown (for X = Br; presumably the unreported complex, $VBr_3(thf)_2(H_2O)$) products.

Although $V(acac)_3$, in contrast, is relatively stable, we found that commercial (both Aldrich and Strem) material "as is" was not suitable for use in any of our physical measurements. HFEPR results obtained from such samples suggested at least two different triplet spin species, which might be attributed to the existence of different crystal structures with slightly different spin Hamiltonian parameters. When $V(acac)_3$ was recrystallized from toluene under nitrogen, HFEPR spectra became much simplified and allowed for a detailed analysis. The same recrystallized material was used in magnetic measurements. VTVH-MCD measurements on commercial material "as is" was even more problematic, suggesting the presence of contaminating $S = 1/2$ species, presumably V(IV). Thus, the VTVH-MCD studies and corroborative HFEPR studies used $V(acac)_3$ synthesized by the convenient and effective method reported by Dilli and Patsalides,[47] which has also been used to prepare a variety of V(III) diketonate complexes.[2] As seen by VTVH-MCD, the synthetic $V(acac)_3$ is free of such contaminants; however, we must assume that the two crystalline forms, α and β,[26] are both present in our synthetic samples, as well as in the commercial material.

EPR Spectroscopy. HFEPR spectra were recorded on two separate instruments. One HFEPR spectrometer employs a superconducting magnet (0−17 T) and has been previously described in detail.[48] The other HFEPR spectrometer is part of the new submm facility at NHMFL.[49] Tunable frequencies in the 150−700 GHz range (~5−23 cm^{-1} energy) were provided by a set of four BWOs (Institute of General Physics, Moscow, Russian Federation). The high-voltage power supply and the permanent magnet housing for the tubes were acquired from the same source. The frequency was precalibrated using a Fabry−Perot resonator. The magnet used was the resistive "Keck" magnet (0−25 T) of improved homogeneity (12 ppm in 1 cm diameter spherical volume) and temporal stability. The field was precalibrated using an NMR probe and was checked during the experiment using a DPPH marker. The oversized-pipes wave propagation system was home-built along the principles outlined before.[48] Detection was provided with an InSb hot-electron bolometer (QMC Ltd., Cardiff, U.K.). Modulation for detection purposes was provided alternatively by modulating the magnetic field (1 kHz frequency, 1 mT maximum amplitude) or by chopping the sub-THz wave beam at ca. 300 Hz. A Stanford SR830 lock-in amplifier converted the modulated signal to dc voltage.

(29) Hitchman, M. A.; McDonald, R. G.; Smith, P. W.; Stranger, R. *J. Chem. Soc., Dalton Trans.* **1988**, 1393−1395.
(30) Dolder, S.; Spichiger, D.; Tregenna-Piggott, P. L. W. *Inorg. Chem.* **2003**, *42*, 1343−1349.
(31) Tregenna-Piggott, P. L. W.; Best, S. P. *Inorg. Chem.* **1996**, *35*, 5730−5736.
(32) Landry-Hum, J.; Bussière, G.; Daniel, C.; Reber, C. *Inorg. Chem.* **2001**, *40*, 2595−2601.
(33) Piper, T. S.; Carlin, R. L. *Inorg. Chem.* **1963**, *2*, 260−263.
(34) Machin, D. J.; Murray, K. S. *J. Chem. Soc. A* **1967**, 1498−1504.
(35) Johnson, M. K. In *Physical Methods in Bioinorganic Chemistry*; Que, L., Ed.; University Science Books: Sausalito, CA, 2000; pp 233−285.
(36) Solomon, E. I. *Inorg. Chem.* **2001**, *40*, 3656−3669.
(37) Krzystek, J.; Zvyagin, S. A.; Ozarowski, A.; Fiedler, A. T.; Brunold, T. C.; Telser, J. *J. Am. Chem. Soc.* **2004**, *126*, 2148−2155.
(38) Figgis, B. N.; Lewis, J.; Mabbs, F. *J. Chem. Soc.* **1960**, 2480−2485.
(39) Baker, J.; Figgis, B. N. *Aust. J. Chem.* **1980**, *33*, 2377−2385.
(40) McElearney, J. N.; Schwartz, R. W.; Merchant, S.; Carlin, R. L. *J. Chem. Phys.* **1971**, *55*, 466.
(41) Smit, J. J.; van Wijk, H. J.; de Jongh, L. J.; Carlin, R. L. *Chem. Phys. Lett.* **1979**, *62*, 158−160.
(42) Gregson, A. K.; Doddrell, D. M.; Healy, P. C. *Inorg. Chem.* **1978**, *17*, 1216−1219.
(43) Casey, A. T.; Clark, R. J. H. *Inorg. Chem.* **1969**, *8*, 1216−1222.
(44) Sobota, P.; Fritsky, I. O.; Ejfler, J.; Szafert, S.; Glowiak, T. *Polyhedron* **1996**, *15*, 381−384.
(45) Manzer, L. *Inorg. Synth.* **1982**, *21*, 135−139.
(46) Fowles, G. W. A.; Greene, P. T.; Lester, T. E. *J. Inorg. Nucl. Chem.* **1967**, *29*, 2365−2370.
(47) Dilli, S.; Patsalides, E. *Aust. J. Chem.* **1976**, *29*, 2389−2393.
(48) Hassan, A. K.; Pardi, L. A.; Krzystek, J.; Sienkiewicz, A.; Goy, P.; Rohrer, M.; Brunel, L.-C. *J. Magn. Reson.* **2000**, *142*, 300−312.
(49) Zvyagin, S. A.; Krzystek, J.; van Loosdrecht, P. H. M.; Dhalenne, G.; Revcolevschi, A. *Physica B* **2004**, *346−347*, 1−5.

Typically, 30−40 mg of solid sample was used for HFEPR. In previous HFEPR studies of pure solid samples characterized by $S = 2$ and negative D, magnetic field-induced torquing of microcrystallites occurred, so that quasi-single-crystal spectra were obtained at low temperatures.[50−52] In these V(III) complexes, this effect was observed in $VBr_3(thf)_3$ but was much weaker in $V(acac)_3$, with only partial orientation occasionally observed. Attempts to prevent torquing effects by the immobilization procedures used previously (embedding the sample in an *n*-eicosane mull or preparing KBr pellets) were only partly successful. The ideal powder-pattern spectra were thus not achieved for either sample. However, the multifrequency, or tunable-frequency, methodology employed here allowed us to identify particular turning points within the nonideal powder patterns and accurately determine spin Hamiltonian parameters.

EPR Analysis. The magnetic properties of an ion with $S = 1$ can be described by the standard spin Hamiltonian comprised of Zeeman and zfs terms:[53]

$$\mathcal{H} = \beta B \cdot \mathbf{g} \cdot S + D(S_z^2 - S(S+1)/3) + E(S_x^2 - S_y^2) \qquad (1)$$

The canonical resonance field versus sub-THz wave quantum energy dependencies were fitted by using a nonlinear least-squares procedure based on the well-known formulas resulting from the exact solution of the secular equation for the triplet state.[54] Use of only the canonical resonance fields is justified in triplet-state EPR since the observed turning points indeed correspond to the axial orientations (except for the so-called B_{min}). This procedure was used in conjunction with human judgment, which was used to eliminate unphysical but mathematically possible results, to obtain best fit parameters for the entire field vs energy array of EPR transitions for a given complex. The errors in parameters were estimated by using the Hessian matrix method.[55] Individual powder spectra were simulated using exact analytical formulas for the resonance fields for $S = 1$ systems at a random orientation of the magnetic field.[56] Transition probabilities were calculated from the eigenvectors in a standard way.[57] Finally, the calculated transition intensities were corrected for the Boltzmann populations of the levels involved. This was necessary due to the very high values of the zfs parameters and the high magnetic fields at which certain transitions occurred.

Optical Measurements and Analysis. Solid samples of the three V(III) complexes were prepared as uniform mulls in poly(dimethylsiloxane) (Aldrich). All sample preparations were performed under anaerobic conditions in a glovebox. Electronic absorption and variable-temperature variable-field MCD spectra were measured using a Jasco J-715 spectropolarimeter in conjunction with an Oxford Instruments SM-4000 8T magnetocryostat. VTVH-MCD data were analyzed using the software program developed by Dr. Frank Neese (MPI Mülheim, Mülheim, Germany).[58,59] For $V(acac)_3$ and $VBr_3(thf)_3$, the VTVH-MCD curves were fit using the spin-Hamiltonian parameters determined by HFEPR, allowing only the band polarizations to vary. For $VCl_3(thf)_3$, the zfs parameters were systematically varied over the ranges of $1 < |D| < 12$ cm^{-1} and $0 < E/D < 0.33$ to locate the best overall fits of the three VTVH-MCD data sets collected at 482, 525, and 742 nm. For each set of zfs parameters the three transition moment products (M_{xy}, M_{xz}, and M_{yz}) were adjusted to achieve the best agreement between the experimental and calculated data, as expressed by the goodness-of-fit parameter (χ^2):

$$\chi^2 = \sum_{i=1}^{N} (f_i^{(calc)} - f_i^{(exp)})^2$$

The χ^2 values from the three data sets were summed to obtain the composite goodness-of-fit ($\Sigma\chi^2$).

Magnetic Measurements and Analysis. Bulk magnetization measurements were obtained from a standard Quantum Design MPMS2 SQUID magnetometer. The samples consisted of randomly oriented microcrystals with a total mass of 119.1 mg for $VCl_3(thf)_3$, 166.1 mg for $VBr_3(thf)_3$, and 155.5 mg for $V(acac)_3$ placed in gel cap sample holders and immobilized in *n*-eicosane. Temperature-dependent magnetic susceptibility measurements were run from 5 to 300 K at a magnetic field of 0.1 T. Magnetization versus field measurements were performed at multiple temperatures and at magnetic fields of 0.1, 1, 2.5, 3.5, 4.5, and 5.5 T.

A blank consisting of a gel cap and eicosane was measured under the same experimental conditions so that the background signal could be subtracted from the data. The experiment uncertainty arising from the sample holder and SQUID itself contribute a maximum of 2×10^{-5} emu/mol in the high-temperature region ($T \gtrsim 40$ K).

The diamagnetic contribution of each sample, estimated from Pascal's constants,[60] $\chi_D = -244.15 \times 10^{-6}$ emu/mol for $VCl_3(thf)_3$, $-274.15\ 10^{-6}$ emu/mol for $VBr_3(thf)_3$, and -166.0×10^{-6} emu/mol for $V(acac)_3$, was then subtracted from each background corrected value to yield the paramagnetic molar susceptibility, χ_P. The resulting values of the susceptibility were compared to the theoretical expectations in the high-temperature limit, i.e., near 300 K.

Field-dependent magnetization and temperature-dependent magnetic susceptibility data were fit by use of the locally written programs DMAGFITP and DSUSFITP,[61] respectively, which employ the Hamiltonian in eq 1 assuming an isolated ground spin state and collinear **D** and **g** matrixes, where the **g** matrix can be isotropic, axial, or rhombic. True powder averages in three dimensions are calculated. The value of D can be constrained as positive or negative, and both cases were explored; the value of E is constrained to $|E| \leq |D/3|$. A least-squares minimization using experimental data from all fields and temperatures simultaneously optimizes the calculated D, E, and g values. Error associated with these parameters was estimated using the standard deviations of several fits with very similar goodness-of-fit values.

Ligand-Field Analysis. Data for the V(III) complexes were analyzed using two programs in tandem: the program LIGFIELD,

(50) Goldberg, D. P.; Telser, J.; Krzystek, J.; Montalban, A. G.; Brunel, L.-C.; Barrett, A. G. M.; Hoffman, B. M. *J. Am. Chem. Soc.* **1997**, *119*, 8722−8723.
(51) Krzystek, J.; Telser, J.; Pardi, L. A.; Goldberg, D. P.; Hoffman, B. M.; Brunel, L.-C. *Inorg. Chem.* **1999**, *38*, 6121−6129.
(52) Krzystek, J.; Telser, J.; Hoffman, B. M.; Brunel, L.-C.; Licoccia, S. *J. Am. Chem. Soc.* **2001**, *123*, 7890−7897.
(53) Abragam, A.; Bleaney, B. *Electron Paramagnetic Resonance of Transition Ions*; Dover Publications: New York, 1986.
(54) Kottis, P.; Lefebvre, R. *J. Chem. Phys.* **1964**, *41*, 379−393.
(55) Press, W. H.; Flannery, B. P.; Teukolsky, A. A.; Vetterling, W. T. In *Numerical Recipes in Pascal*; Cambridge University Press: Cambridge, U.K., 1989; p 572.
(56) Baranowski, J.; Cukierda, T.; Jezowska-Trzebiatowska, B.; Kozlowski, H. *Chem. Phys. Lett.* **1976**, *39*, 606−608.
(57) Bencini, A.; Gatteschi, D. In *Transition Metal Chemistry*; Melson, G. A., Figgis, B. N., Eds.; Marcel Dekker: New York, 1982; Vol. 8, p 1.
(58) Neese, F.; Solomon, E. I. *Inorg. Chem.* **1999**, *38*, 1847−1865.
(59) The software is available from Dr. F. Neese, MPI Mülheim, Mülheim, Germany.
(60) O'Connor, C. J. *Prog. Inorg. Chem.* **1982**, *29*, 203−283.
(61) Krzystek, J.; Yeagle, G.; Park, J.-H.; Meisel, M. W.; Britt, R. D.; Brunel, L.-C.; Telser, J. *Inorg. Chem.* **2003**, *42*, 4610−4618.

written by J. Bendix,[62] and a locally written program, DDN. LIGFIELD is an extremely versatile and powerful program that can use any d orbital basis set in ligand-field calculations and parametrizes the d orbital energies using either a crystal-field or angular overlap model (AOM)[63] approach. Both programs employed the entire basis set (45 microstates) for d^2 and provided eigenvalues (energy levels) for comparison with experimental zfs and optical transitions. The program DDN uses a crystal-field model (parameters *Dq*, *Ds*, and *Dt* as defined by Ballhausen[64]) or AOM parameters and was also modified by combination with a fitting routine, as with the magnetic analysis programs, to allow fitting of triplet−triplet electronic transitions by varying ligand-field parameters.

Calculation of *g* values was done using the following equations, similar to those of Gregson et al.,[42] but adapted for rhombic symmetry:

$$g_z = [(\epsilon_{3z} - \epsilon_{2z})^2 - (2E)^2]^{1/2}/(2\beta B_z) \quad (2a)$$

$$g_{x,y} = [(\epsilon_{3x,y} - \epsilon_{1x,y})^2 - (D + E)^2]^{1/2}/(2\beta B_{x,y}) \quad (2b)$$

Here $D = [(1/2)(\epsilon_3 + \epsilon_2) - \epsilon_1]$ and $E = (1/2)(\epsilon_3 - \epsilon_2)$ and the quantities ϵ_{il}, where $i = 1-3$ and $l = x, y, z$, or none for zero-field, are the three lowest energy eigenvalues, in ascending order, in our case, of the 45 × 45 matrix including all of the interelectronic, ligand-field, and spin−orbit (including the Stevens reduction factor, *k*) terms, plus Zeeman terms with an external magnetic field applied along either the *x*, *y*, or *z* direction (as defined by the ligand-field coordinate system).[65] These three eigenvalues are then related to the three analytical solutions of the 3 × 3 spin Hamiltonian matrix for $S = 1$ with rhombic zfs and **g** matrix and arbitrary field magnitude along either the *x*, *y*, or *z* direction. Calculations were made using fields applied in each of the *x*, *y*, and *z* directions over the range 0−4 T.

In addition, analytical equations for triplet state energy levels were used, as done by Gregson et al.[42] These equations were taken from an early optical analysis of V(III) in corundum by Pryce and Runciman[7,66] These equations were also combined with a fitting program to yield best fit parameters for *B*, *Dq*, and *υ*, for comparison with exact solution results.

Results

HFEPR Spectroscopy of V(acac)$_3$. A HFEPR spectrum of polycrystalline $V(acac)_3$ consists of no more than two transitions at any given frequency (Figure 1), except in two narrow ranges around 180 and 285 GHz, where three signals are observed. The omnipresent signal at $g \sim 1.9$, which is attributable to a V(IV) impurity (not shown), is discounted. The shape of the spectra suggests artifacts due to partial torquing; it is possible however to simulate an approximate powder pattern using the parameters indicated in the caption to Figure 1. A much better line shape agreement between the simulated and experimental spectra is obtained for a positive value of *D* than for a negative one. A two-dimensional resonance field versus energy data set of $V(acac)_3$ was collected and is shown in Figure 2 as squares. The resonances thus plotted form characteristic branches that are easily recognizable and labeled according to the standard terminology for triplet spin states of rhombic symmetry.[54,67] Cross-sections along the field axis in Figure 2 correspond to individual HFEPR spectra such as in Figure 1. In the case of possible artifacts, such as the doubling of the 10.5 T signal at 326 GHz (see Figure 1), we took an average position of the signals as the resonance field. Two zero-field resonances were detected, at ca. 167 and 281 GHz (5.57 and 9.37 cm^{-1}, respectively), which could be attributed alternatively to either the $2|E|$ and $|D| - |E|$ or $|D| - |E|$ and $|D| + |E|$ transitions within the triplet manifold. The third zero-field transition should then lie at either ca. 12.2 or 3.8 cm^{-1}, respectively. The first of these two values, corresponding to a frequency of 366 GHz, is well within the frequency range of our tunable sources, but we could not detect any absorption at that frequency. The lower value, equal to 114 GHz, is outside

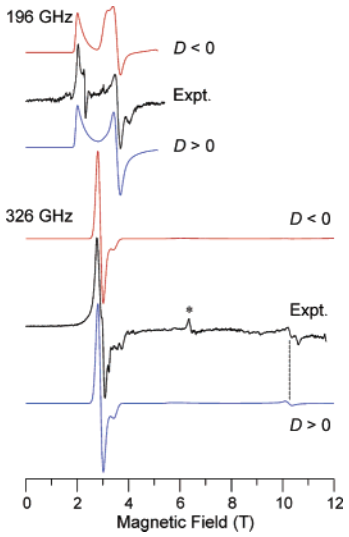

Figure 1. Representative HFEPR spectra of polycrystalline $V(acac)_3$ at two different frequencies. Top layer: $\nu = 196.18$ GHz, with simulations for negative *D* (red) and for positive *D* (blue). Bottom layer: $\nu = 325.76$ GHz, with simulations for positive and negative *D*, as labeled. Experimental conditions: temperature, 5 K; field sweep rate, 0.5 T/min; field modulation frequency, 8.1 kHz; modulation amplitude, 1.6 mT; time constant, 0.3 s. Sub-THz wave power strongly dependent on frequency. Simulation parameters for both frequencies: $|D| = 7.65$ cm^{-1}; $|E| = 1.99$ cm^{-1}; $g_x = 1.84$; $g_y = 1.80$; $g_z = 1.84$. Single-crystal Gaussian line widths assumed in the simulations: 180 mT for the *x* and *z* turning points; 100 mT for the *y* turning point. The line at 6.42 T at 326 GHz (indicated by an asterisk) originates from the fourth harmonic of the fundamental frequency and is not reproduced in the simulation. A guideline is included in the spectrum at 325.76 GHz to indicate the experimental signal that is present only in the simulation with $D > 0$.

(62) Bendix, J.; Brorson, M.; Schäffer, C. E. *Inorg. Chem.* **1993**, *32*, 2838−2849.
(63) Schäffer, C. E. *Struct. Bonding* **1968**, *5*, 68−95.
(64) Ballhausen, C. J. In *Introduction to Ligand Field Theory*; McGraw-Hill: New York, 1962; pp 99−103.
(65) For $D < 0$, the state ordering is reversed, so that $D = [(1/2)(\epsilon_1 + \epsilon_2) - \epsilon_3]$ and $E = (1/2)(\epsilon_1 + \epsilon_2)$; eq 2a is then $g_z = [(\epsilon_{1z} - \epsilon_{2z})^2 - (2E)^2]^{1/2}/(2\beta B_z)$, and eq 2b is unchanged.
(66) These equations are as follows: $\Delta E(^3T_2 - {}^3T_1(F)) = 10Dq - E_-$ and $\Delta E(^3T_1(P) - {}^3T_1(F)) = E_+ - E_-$, where $E_\pm = (1/2)[15B + 10Dq \pm \{(15B)^2 + 18B{\cdot}10Dq + (10Dq)^2\}^{1/2}] \approx 15B + 10Dq$, and 0, respectively. These equations give identical results to an exact calculation for octahedral symmetry, in the absence of spin−orbit coupling. Trigonal distortion leads to a diagonal term, *υ*, so that the $^3T_1(F)$ ground-state splits into $^3A_2$ at $-(2/3)\upsilon$ and ^3E at $+\upsilon$; the $^3T_{1(2)}$ excited states split into $^3A_{2(1)}$ at $-\upsilon/3$ and ^3E at $+\upsilon/6$. There is also an off-diagonal trigonal term, υ', which we and Gregson et al.[42] ignore; its effect on the energy levels is minor for small *υ*, and in any case, our exact calculations take it into account.
(67) Wasserman, E.; Snyder, L. C.; Yager, W. A. *J. Chem. Phys.* **1964**, *41*, 1763−1772.

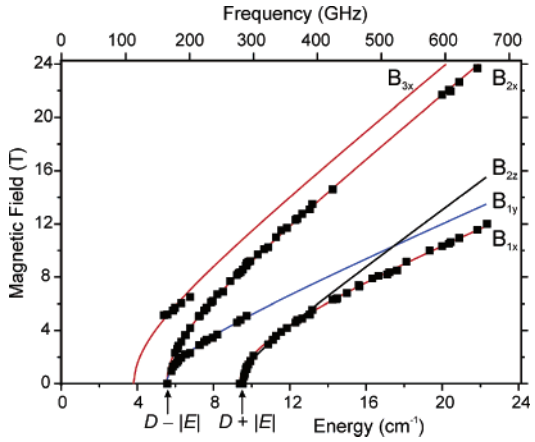

Figure 2. Resonant field vs quantum energy dependence of polycrystalline $V(acac)_3$ at 10 K. The squares are experimental HFEPR points while the curves were simulated using the following spin Hamiltonian parameters: $S = 1$; $D = +7.470$ cm^{-1}; $E = +1.916$ cm^{-1}; $g_x = 1.833$; $g_y = 1.72$; $g_z = 2.03$. The particular transition branches are identified using standard nomenclature for triplet states with rhombic symmetry.[54,67] Simulations are shown by red lines for *x* turning points, blue lines for *y* turning points, and black lines for *z* turning points. The two observable zero-field resonances are also labeled accordingly. Additional features due to a minor species were observed but are not shown (see text).

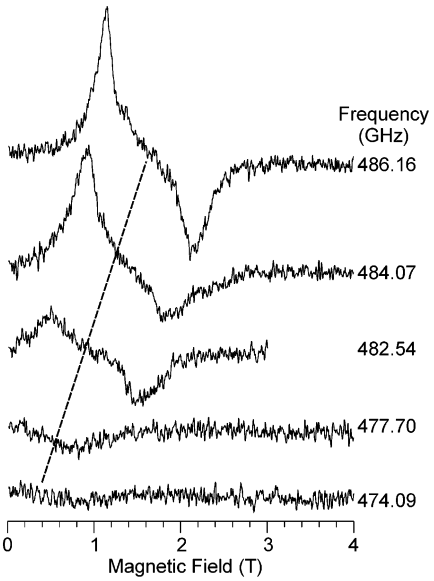

Figure 3. HFEPR spectra of $VCl_3(thf)_3$ at different frequencies at 4.5 K. Other experimental conditions are as in Figure 1. A guideline traces the resonance to zero-field resonance at ca. 474 GHz = 15.8 cm^{-1}.

our range, but we did detect resonances attributed to the B_{3x} turning point of the powder spectrum, which extrapolate a zero-field frequency value of about 110 GHz (Figure 2). We therefore attribute the observed zero-field absorptions to $|D| - |E|$ and $|D| + |E|$ transitions, which yield immediate approximate zfs values of $|D| \approx 7.45$ and $|E| \approx 1.9$ cm^{-1}. The previous magnetic susceptibility study of this complex[42] is in good agreement with this estimate for *D*.

To accurately determine the spin Hamiltonian parameters responsible for the $V(acac)_3$ HFEPR spectra, we performed a simultaneous nonlinear least-squares fit involving the entire experimental data set (see Experimental Section). This automated fitting procedure yielded the following: $D = +7.470(1)$ cm^{-1}; $E = +1.916(1)$ cm^{-1}; $g_x = 1.833(4)$; $g_y = 1.72(2)$; $g_z = 2.03(2)$.[68] Although these values are somewhat different from those in the single-frequency simulations presented in Figure 1, they better represent the spin system of interest by virtue of providing suitable fits for all frequencies at which data were collected.[69] The value for g_z (2.03) is not fully reliable since it is based on a fit to only three points at very low fields attributed to the B_{2z} transition branch, but which may instead belong to the B_{1x} branch. Generally, values below g_e are expected for V(III), a less than half-filled 3d electron system.[53] Some observed lines, such as the upper line at ca. 10.5 T at 326 GHz (Figure 1, lower layer), are split into two signals. It is not certain whether this effect is intrinsic or due to torquing effects, as the simulations reproduce only the lower-field signal. Reproduction of the upper-field signal would require a slightly different set of spin Hamiltonian parameters. The simulations, however, confirm the positive sign of *D*, since only for positive *D* does that particular line appear at low temperatures (see Figure 1).

Even though a single-crystal HFEPR study of magnetically isolated V(III) in axial symmetry did observe well-resolved hyperfine splitting for ^{51}V ($I = 7/2$, 100% abundance),[25] we note that no resolved hyperfine splitting was detected in $V(acac)_3$ nor in either of the two thf complexes. It is likely that our failure to observe ^{51}V hyperfine splitting is primarily a consequence of dealing with a magnetically nondilute system. Attempts to observe HFEPR spectra of the three V(III) complexes in frozen solution were unsuccessful. We note, however, that we have never observed ^{55}Mn ($I = 5/2$, 100% abundance) hyperfine splitting in frozen solution HFEPR spectra of axial or rhombic $S = 2$ complexes.[70−72]

HFEPR Spectroscopy of $VCl_3(thf)_3$. HFEPR spectra at 4.5 K of polycrystalline $VCl_3(thf)_3$ at several, closely spaced, sufficiently high sub-THz frequencies are presented in Figure 3. At 486 GHz two signals are clearly visible that converge into a single line with decreasing frequency, so that at about 474 GHz (15.8 cm^{-1}) a single zero-field transition can be extrapolated, although its broadness precludes direct detec-

(68) Since the sign of *E* could not be determined, we assumed it to be the same as the sign of *D* for all investigated complexes. This affects the attribution of perpendicular turning points in Figure 2 to the *x* and *y* axes and, consequently, also the attribution of g_x and g_y values. For a sign of *E* opposite to that of *D*, the g_x and g_y values must be exchanged.

(69) In addition to the HFEPR signals shown in Figure 1 and plotted in Figure 2, we also observed resonances whose intensity depended on the sample preparation history. From their field/energy dependencies (not shown) it could be concluded that they represent another triplet spin species with spin Hamiltonian parameters somewhat different from the "majority species" described in detail above. It was not possible, however, to extract precise values of those parameters. Since in the most carefully prepared HFEPR samples the intensity of these "extra resonances" was negligible, we conclude that they represent a "minority species" that needs not be considered in EPR analysis.

(70) Krzystek, J.; Pardi, L. A.; Brunel, L.-C.; Goldberg, D. P.; Hoffman, B. M.; Licoccia, S.; Telser, J. *Spectrochim. Acta, Part A* **2002**, *58*, 1113−1127.

(71) Krzystek, J.; Telser, J. *J. Magn. Reson.* **2003**, *162*, 454−465.

(72) The observation of resolved ^{51}V hyperfine coupling in alums[25] might also have been assisted by the rigorously axial symmetry of that system. In multifrequency EPR studies of high-spin Mn(II), we have found that simulations including a small magnitude of rhombic zfs (e.g., $|E/D| < 0.1$) can effectively broaden the $M_S = \pm 5/2 \leftrightarrow \pm 3/2$ EPR transitions (although not the $\pm 1/2$ transition). Distribution in *E* is also expected to have a further deleterious effect on resolution.

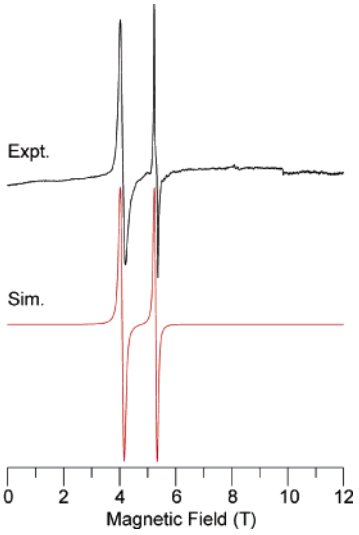

Figure 4. Experimental (black trace) and simulated (red trace) HFEPR spectra of $VBr_3(thf)_3$ at 336.57 GHz and at 10 K. The simulation used spin Hamiltonian parameters as in Table 1, with the assumption of a single-crystal-like spectrum with the *z* zfs axis aligned parallel to the Zeeman field. Single-crystal line widths (50% Gaussian, 50% Lorentzian) assumed in the simulation: 100 mT (parallel turning points); 140 mT (perpendicular turning points). The presence of B_1 fields of equal amplitude both parallel and perpendicular to B_0 was also assumed.

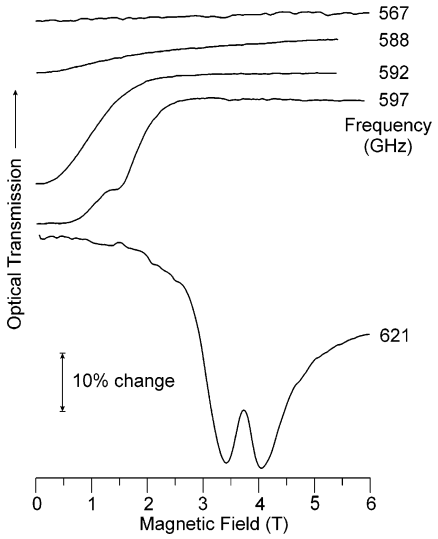

Figure 5. HFEPR spectra of $VBr_3(thf)_3$ at 7 K. The spectra were obtained using a tunable-frequency source (BWO) employing optical modulation of the sub-mm wave beam. This results in the resonance being detected as a decrease of sub-mm wave transmission through the sample. A bar indicates the signal intensity corresponding to 10% transmission. Experimental conditions: optical modulation frequency, 280 Hz; magnetic field sweep rate, 1 T/min.

tion. The convergence of different signals into a single zero-field transition is typical for the different turning points of a rhombic triplet powder pattern, which collapse into one of three isotropic absorptions in the absence of magnetic field. Since no additional transitions are observable in $VCl_3(thf)_3$, it is not possible to determine directly which of these three zero-field transitions is detected at 474 GHz, but by comparison with the results of magnetic and MCD studies (see below), it is most likely the $|D| + |E|$ transition. Note that, in the case of maximum rhombicity ($|E/D| = 1/3$), there are only two zero-field resonances, situated at $|D| - |E| = |2E| = (2/3)|D|$, and at $|D| + |E| = (4/3)|D|$. If this assumption is valid for $VCl_3(thf)_3$, then it is possible to estimate zfs parameters from the single observable zero-field resonance, yielding $|D| = 11.85$ and $|E| = 3.95$ cm^{-1}. It is obviously impossible to determine *g* values from HFEPR for this complex.

HFEPR Spectroscopy of $VBr_3(thf)_3$. HFEPR spectra of polycrystalline $VBr_3(thf)_3$ were first collected using the Gunn oscillator-based multifrequency spectrometer. A representative spectrum is shown in Figure 4 together with the corresponding simulation. Under visual inspection, the spectrum does not correspond to a powder pattern. Indeed, the simulations were successful only when a strong field-induced orientation of the crystallites was assumed along the *z* axis of the zfs tensor. This torquing effect was sample-dependent and not always present to the same degree. In addition, the simulations required the presence of a B_1 component of comparable amplitude parallel to the B_0 field. Although the spectrometer configuration is such that B_1 is nominally perpendicular to B_0, the presence of the parallel field component can be attributed to multiple reflections and general imperfections (mode impurity) of the sub-THz wave propagation system employed.

The use of multiple frequencies generated by the Gunn oscillators allowed us to detect a zero-field resonance at ca. 222 GHz (7.4 cm^{-1}). The presence of a second zero-field resonance at ca. 375 GHz (12.5 cm^{-1}) could be deduced by extrapolating other observable transitions to zero field. The frequency of the third zero-field transition could not be established. We thus took advantage of our recently introduced method of gathering tunable-frequency HFEPR data using BWO sources.[73] Figure 5 depicts spectra recorded at several frequencies in the vicinity of 600 GHz. Instead of the usual modulation of magnetic field, we modulated the sub-THz wave beam. In such a case, the resonance is detected as a decrease of transmission through the sample, as in standard optical spectroscopy. A zero-field feature is clearly visible at ca. 592 GHz (19.7 cm^{-1}) that develops into a resonance with at least two components as the frequency and corresponding resonant field is slightly increased. The energy of this transition is approximately the sum of the two previously mentioned resonances, which unequivocally establishes that the transition at ca. 19.7 cm^{-1} is the $|D| + |E|$ zero-field resonance, the one at ca. 12.5 cm^{-1} is the $|D| - |E|$ resonance, and the one at ca. 7.4 cm^{-1} is the $2|E|$ resonance.

The full resonance field vs sub-THz wave quantum energy data set for $VBr_3(thf)_3$ is plotted in Figure 6 as squares**.** The three observed zero-field transitions yield an immediate estimate of the values of the zfs parameters: $|D| \approx 16$; $|E| \approx 3.7$ cm^{-1}. The spin Hamiltonian parameters were subsequently best-fitted to the experimental resonances using the automated procedure previously described. The sign of *D* was found to be negative from variable-temperature single-frequency HFEPR experiments (not shown) and other

(73) Zvyagin, S. A.; Krzystek, J.; van Loosdrecht, P. H. M.; Dhalenne, G.; Revcolevschi, A. *Phys. Rev. B* **2003**, *67*, 212403.

Table 1. Spin Hamiltonian Parameters for V(III) Complexes As Determined by Magnetic Resonance and Magnetic Susceptibility Measurements

complex	method, ref	D (cm^{-1})[a]	E (cm^{-1})[a]	$g_\perp$ (g_x, g_y)	$g_\parallel$ (g_z)
$V(acac)_3$	HFEPR, this work[b]	+7.470(1)	+1.916(1)	1.833(4), 1.72(2)	2.03(2) (g_{iso} 1.86)
	magn, this work[c]	+7.4(1)	2.4(1)	1.7	1.7
	magn[42]	+7.7		1.78	1.96 (g_{iso} 1.84)
$VCl_3(thf)_3$	HFEPR, this work[d]	11.85	3.95		
	VTVH-MCD, this work[b]	−10(3)	1.6(4)	1.8	1.8
	magn, this work[c]	11−14	3−4	1.7(1)	1.7(1)
$VBr_3(thf)_3$	HFEPR, this work[b]	−16.162(6)	−3.694(4)	1.86(1), 1.90(1)	1.710(4)
	magn, this work[e]	−16.2(2)	−3.9(1)	1.75(5)	1.75(5)
V^{3+}:Al_2O_3[f]	EPR,[8,9] HFEPR,[14] far-IR[15]	7.85	<0.01		1.915
		8.29			1.910
		8.25		1.74	1.92
V^{3+}:[CsGa alum][g]	HFEPR[25]	+4.8581	0	1.8656	1.9500
V^{3+}:[RbV alum][h]	HFEPR[24]	+4.906	0	1.863	1.944
$Cs_3VCl_6{\cdot}4H_2O$	magn[41]	7.85		1.80	1.94
GVSH[i]	magn[40]	3.74		1.66	1.94

[a] Signs of zfs parameters are given where they have been definitively determined. The sign of E is related to the choice of g_x vs g_y in the HFEPR analysis; it cannot be determined by VTVH-MCD. [b] Use of the parameters determined by HFEPR for $V(acac)_3$ and $VBr_3(thf)_3$ fitted the VTVH-MCD data within experimental error. Independent fits of the VTVH-MCD data for $VCl_3(thf)_3$ were made. [c] Parameters determined by variable-temperature powder magnetic susceptibility. [d] Parameters for $VCl_3(thf)_3$ have been derived under assumption of maximum rhombicity ($|E/D| = 1/3$). [e] Parameters given are a consensus of those determined for powder samples by both field-dependent magnetization at multiple temperatures and by variable-temperature dc magnetic susceptibility. [f] V(III) as a dopant in single-crystal corundum (Al_2O_3). A combination of values from the two conventional frequency (ν < 94 GHz) EPR studies[8,9] is given. Values determined by HFEPR[14] and by far-IR absorption[15] are listed separately. [g] V(III) as a dopant in single-crystal $CsGa(SO_4)_2C12H_2O$, wherein the V(III) is found as $[V(H_2O)_6]^{3+}$. The D_2O complex was also studied and gave $D = 4.7735$ cm^{-1}, $g_\perp = 1.8690$, and $g_\parallel = 1.9549$. [h] $RbV(SO_4)_2{\cdot}12H_2O$, wherein the V(III) is found as $[V(H_2O)_6]^{3+}$. [i] Single-crystal guanidinium vanadium sulfate hexahydrate, $[C(NH_2)_3]V(SO_4)_2{\cdot}6H_2O$. X-band EPR spectra of V^{3+}:GASH (V(III) as a dopant in $[C(NH_2)_3]Al(SO_4)_2{\cdot}6H_2O$) gave $g_\parallel = 1.86$,[10] which value in combination with the magnetic data gave $D = 3.59$ cm^{-1} and $g_\perp = 1.64$.[40]

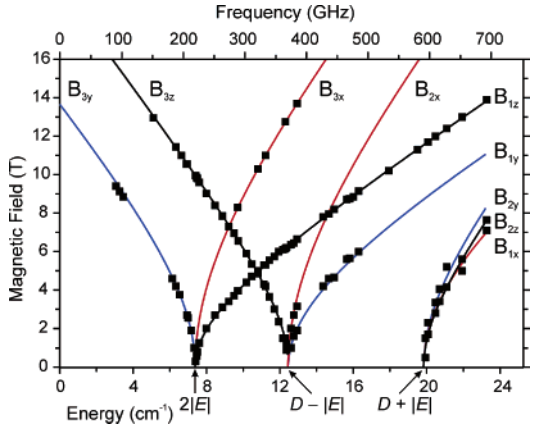

Figure 6. Resonant field vs quantum energy dependence of polycrystalline $VBr_3(thf)_3$ at 10 K. The squares are experimental HFEPR points while the curves were simulated using the following best-fit spin Hamiltonian parameters: $S = 1$; $D = -16.162$ cm^{-1}; $E = -3.694$ cm^{-1}; $g_x = 1.86$; $g_y = 1.90$; $g_z = 1.71$. The particular transition branches are identified using standard nomenclature for triplet states with rhombic symmetry.[54,67] Simulations are shown by red lines for x turning points, blue lines for y turning points, and black lines for z turning points. The three observable zero-field resonances are also labeled accordingly.

evidence.[74] The final values of the spin Hamiltonian parameters are thus the following: $D = -16.162(6)$ cm^{-1}; $E = -3.694(4)$ cm^{-1} ($|E/D| = 0.229$); $g_x = 1.86(1)$; $g_y = 1.90(1)$; $g_z = 1.710(4)$ (Table 1).[75]

(74) The negative sign of D can be also drawn from the following thermodynamics argument: for $D > 0$, the two uppermost triplet spin sublevels τ_x and τ_y lie above the lowest level τ_z. In the case of large $|D|$, only the τ_z level is thus significantly populated at low temperatures, so the $|D| - |E|$ and $|D| + |E|$ transitions, which originate from the τ_z level, are observed but not the $2|E|$ transition. This is the case in $V(acac)_3$. In $VBr_3(thf)_3$, however, all three zero-field transitions are observed at low temperature, which is possible only when the τ_x and τ_x levels lie lower in energy than τ_z, i.e., $D < 0$.

(75) A "minority species" was observed in HFEPR spectra of $VBr_3(thf)_3$ analogous to the situation with $V(acac)_3$.[69]

Magnetic Circular Dichroism Measurements. As described above, no optical spectroscopic data have previously been reported for $VBr_3(thf)_3$, and the electronic absorption spectra for both $VCl_3(thf)_3$[34] and $V(acac)_3$[33,34] merit reinvestigation with MCD spectroscopy, which is a complementary and considerably more sensitive tool. The solid-state electronic absorption spectra at 4 K of these three compounds in the range of 300−625 nm are shown in Figure S1 (Supporting Information). For both $VCl_3(thf)_3$ and $V(acac)_3$, these low-temperature absorption spectra are fully consistent with the previously reported spectral data.[34] $VBr_3(thf)_3$ exhibits three intense peaks between 21 000 and 32 000 cm^{-1}, along with a weak shoulder at 18 800 cm^{-1}.

$V(acac)_3$ has been reported to exhibit absorption features at 18 180 and 21 740 cm^{-1} (550 and 460 nm, respectively), with the single-crystal data[33] providing little improvement over solution data,[34] either in resolution or in assigning the polarizations of the transitions. Far more informative are the MCD spectra of $V(acac)_3$ shown in Figure 7a. Since MCD selection rules require spin−orbit coupling among states for signal intensity, the most intense MCD bands are those involving the metal d-orbitals, such as ligand field (LF) and charge-transfer (CT) transitions. Consequently, the acac-based $\pi \rightarrow \pi^*$ transitions that dominate the electronic absorption spectrum of $V(acac)_3$ are relatively weak in the MCD spectrum and collectively form a broad, positive feature from ∼15 000 to 27 000 cm^{-1}. In contrast, the LF transitions give rise to very intense MCD bands and primarily appear as negative features superimposed on the positive background provided by the acac $\pi \rightarrow \pi^*$ transitions. The two LF transitions observed at 18 200 and 21 100 cm^{-1} correspond to the two absorption features reported previously.[33,34] To higher energy, additional LF bands are apparent in the positive feature at 27 400 cm^{-1} and in the negative bands at 29 700 and 32 600 cm^{-1}.

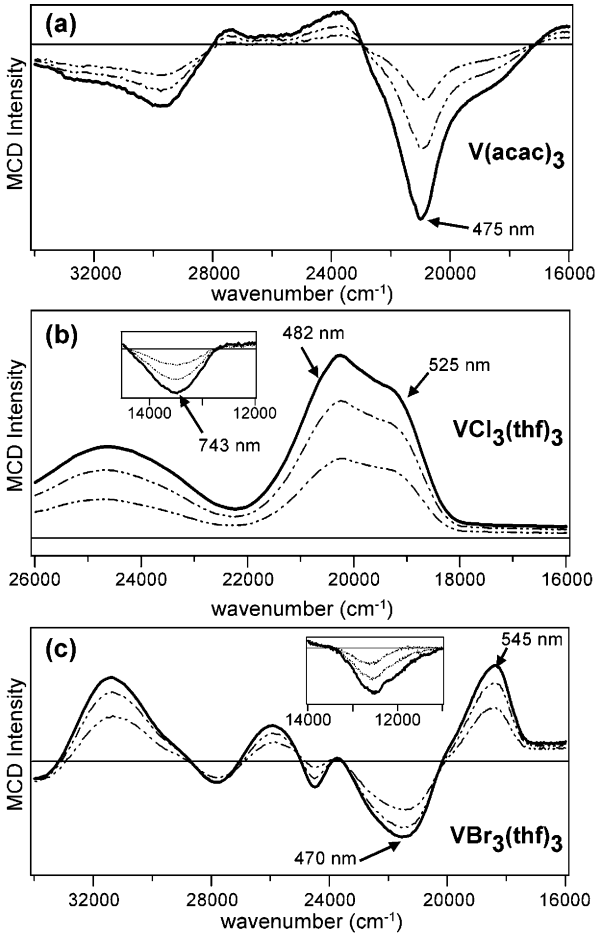

Figure 7. Variable-temperature solid-state MCD spectra of $V(acac)_3$ (a), $VCl_3(thf)_3$ (b), and $VBr_3(thf)_3$ (c). Spectra were recorded at a magnetic field of 7 T and at temperatures of 4 K (solid line) and 8 and 15 K (dotted lines). MCD intensities increase with decreasing temperature, characteristic of *C*-term behavior. Insets: Near-IR MCD data obtained at the same temperatures. The arrows indicate wavelengths at which VTVH-MCD data were collected.

In comparison to the analysis of the $V(acac)_3$ MCD spectrum discussed above, interpretation of the MCD spectrum of $VCl_3(thf)_3$ shown in Figure 7b is simplified by the lack of interfering ligand-based or CT transitions. Two LF bands are observed at 13 500 and ~20 000 cm^{-1}, corresponding to the weak absorption features previously reported at 12 900 and 20 120 cm^{-1}.[34] Our MCD data reveal that the band at 20 000 cm^{-1} is actually composed of two transitions with a splitting of ~900 cm^{-1}. Halide-to-V(III) CT transitions are found at energies >22 000 cm^{-1} for $VCl_3(thf)_3$ but shift to lower energy in the $VBr_3(thf)_3$ spectrum, making it difficult to distinguish between the LF and CT bands for the latter complex (see Figure 7c). Despite this complication, it is possible to assign the bands of $VBr_3(thf)_3$ on the basis of their relative intensities in the absorption and MCD spectra (*C*/*D* ratios). The band at 18 500 cm^{-1} is intense in the MCD spectrum and weak in the absorption spectrum, suggestive of a LF transition, while the band at 21 600 cm^{-1} carries considerably greater absorption intensity, indicating primarily CT character. An additional LF transition appears in the near-IR region at 12 600 cm^{-1}.

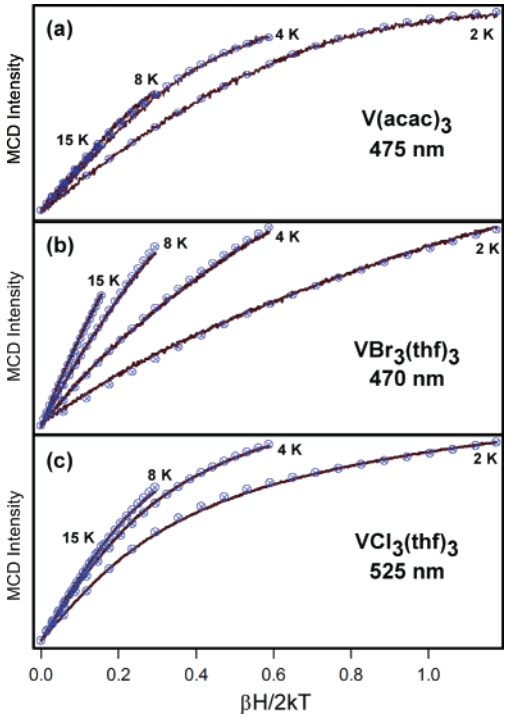

Figure 8. Experimental VTVH-MCD data collected at the indicated wavelengths for $V(acac)_3$ (a), $VBr_3(thf)_3$ (b), and $VCl_3(thf)_3$ (c). Data were obtained at 2, 4, 8, and 15 K with magnetic fields ranging from 0 to 7 T. For $V(acac)_3$ and $VBr_3(thf)_3$, the theoretical fits (⊗) were generated with the spin Hamiltonian parameters determined with HFEPR (Table 1). For $VCl_3(thf)_3$, the fits were obtained using the "best-fit" zfs values of $D = -9.85$ cm^{-1} and $E/D = 0.15$ (with $g_{iso} = 1.8$).

VTVH-MCD data were collected for the three complexes at the wavelengths indicated by arrows in Figure 7. In these VTVH-MCD experiments, the signal intensity was measured at various fixed temperatures as a function of magnetic field between 0 and 7 T. Figure 8 displays three of the resulting VTVH-MCD data sets (one for each complex), while the remainder are shown in Figure S2. By convention, the curves are plotted against $\beta H/2kT$ and the intensities are normalized. As shown by Neese and Solomon,[58] the VTVH-MCD saturation behavior of a $S > 1/2$ system depends on the spin Hamiltonian parameters (*D*, *E*/*D*, and the three *g* values) as well as the polarization of the monitored transition. Consequently, analysis of VTVH-MCD data provides essentially the same magnetization information as that obtained using a SQUID and affords a complementary means of obtaining the zfs parameters of species that otherwise require study by HFEPR, as we recently demonstrated in a combined HFEPR/MCD study of a high-spin ($S = 3/2$) Co(II) system.[37]

Using software developed by Neese,[59] the VTVH-MCD data for $V(acac)_3$ and $VBr_3(thf)_3$ were fit using the same spin Hamiltonian parameters as determined by HFEPR. As shown in Figure 8a,b, excellent fits are obtained for both $V(acac)_3$ and $VBr_3(thf)_3$ with these HFEPR parameters, demonstrating as before[37] the general agreement between HFEPR and VTVH-MCD with regards to determination of zfs values. For $VBr_3(thf)_3$, the fit obtained with $D = -16.126$ cm^{-1} was better by a factor of 2 than that obtained with $D = +16.126$ cm^{-1}, indicating that the VTVH-MCD data strongly support a negative zfs for this complex.

For $VCl_3(thf)_3$, the situation was not as straightforward, given that HFEPR provided only estimates of the zfs parameters and no information regarding the g values and the sign of D. To locate the best overall fits of the three sets of VTVH-MCD data collected for $VCl_3(thf)_3$ (at 482, 525, and 742 nm, as indicated in Figure 7b), the D and E/D values were systematically varied, and for each set of parameters the three transition moment products (M_{xy}, M_{xz}, and M_{yz}) were adjusted to achieve the best agreement between the experimental and calculated data. With this approach, two separate sets of zfs parameters were found to provide excellent fits of the experimental data. Fits assuming a positive D value yielded $D = +6(2)$ cm^{-1} and $|E/D| = 0.30(3)$ (with $g_{iso} = 1.8$). Yet these zfs values would produce a $|D + E|$ transition at a much lower energy than that of the zero-field transition observed by HFEPR for this complex ($\sim$8 cm^{-1} versus 15.8 cm^{-1}; assignment to $|D - E|$ would be even more unreasonable). This magnitude of D is also in substantial disagreement with that from magnetic measurements described below. However, use of a negative value for D also yielded successful fits with $D = -10(3)$ cm^{-1} and $E/D = 0.16(4)$ (with $g_{iso} = 1.8$), which are in reasonable agreement with the field-dependent magnetization data, $D = -12.6$ cm^{-1} and $E/D = 0.30$ (with $g_{iso} = 1.7$). This choice of VTVH-MCD fit parameters would give $|D + E| \approx 12$ cm^{-1}, which is less than that observed by HFEPR, but given the difficulty of determining the frequency of the true zero-field transition observed for $VCl_3(thf)_3$, this discrepancy is within acceptable limits. The best fit obtained with negative zfs parameters for $VCl_3(thf)_3$ is shown in Figure 8c.

Variable-Temperature Magnetic Susceptibility and Variable-Field Magnetization Measurements. Variable-temperature dc SQUID magnetic susceptibility measurements were made on each of the three compounds of interest. Figure S3 presents these data as effective magnetic moment (μ_{eff}) versus temperature together with various fit lines in each case. Qualitatively, all of the complexes exhibit a sharp decrease in μ_{eff} at low temperature (<50 K), indicative of zfs effects.[60] Quantitative analysis of the susceptibility data for $V(acac)_3$ yielded D values in the range $+(7.0-7.5)$ cm^{-1}, with $g_{iso} \approx 1.7(1)$. This magnitude and sign of D is in good agreement with that from the work of Gregson et al.[42] and from our HFEPR results presented above (Table 1). Thus, only the two thf complexes were studied by field-dependent magnetization, and the results are shown in Figure S4. Qualitatively, the magnetization curves show "nesting" as seen in the analogous VTVH-MCD plots.

The combination of susceptibility and magnetization data for $VCl_3(thf)_3$ yielded $|D|$ values in the range $11-14$ cm^{-1}, with $|E| \approx 4$ cm^{-1} and $g_{iso} \approx 1.8(1)$. Fits with both positive and negative D values are acceptable with the latter favoring the upper end of the range given, although no real discrimination among the parameters can be made. This magnitude of D, however, is in agreement with that estimated from the zero-field transition observed in HFEPR and strongly favors the fit of VTVH-MCD data that requires $D < 0$ (see above). For $VBr_3(thf)_3$, the difference in best fit parameters as a function of sign of D was significant. Fits with $D > 0$ gave $|D|$ in the range $12-14$ cm^{-1} along with nearly maximum rhombicity and $g_{iso} \approx 1.7(1)$. Fits with $D < 0$, however, independently gave zfs parameters in almost exact agreement with those from HFEPR (and thus with VTVH-MCD as well): $D = -16.2(2)$ cm^{-1}; $E = -3.9(1)$ cm^{-1}; $g_{iso} \approx 1.75(5)$.

Discussion

The use of high frequencies and fields succeeds in producing EPR spectra from integer spin systems that are otherwise "EPR silent" using conventional spectroscopy. As in our previous HFEPR study of a triplet spin system involving Ni(II) in pseudotetrahedral complexes,[23] the multifrequency approach was of great use in allowing us to unequivocally assign the observed EPR signals to particular turning points of the powder pattern, even when such a pattern was not perfect. Such a situation often occurs in HFEPR spectroscopy of high-spin transition metal complexes when studied as polycrystalline solids. In the case of the V(III) complexes studied in this work, the combination of multiple frequencies with high magnetic fields allowed us to accurately measure large zfs parameters on the order of $|D| \sim 16$ cm^{-1}, which to the best of our knowledge is the highest such value ever obtained from EPR studies of a triplet spin system.

The use of tunable sub-THz wave sources (BWOs) is a logical extension of the multifrequency approach used so far and proved particularly useful in this case. It allowed us to very accurately pinpoint the zero-field resonances characteristic for a triplet state and also improved the accuracy of the resulting g values. As argued by one of us elsewhere,[76] the procedure that yields the most accurate spin Hamiltonian parameters for a triplet state involves a precise determination of the three resonances in zero field, followed by experiments in a magnetic field. Although the transition metal ion complexes studied here are characterized by zfs values that are 2 orders of magnitude larger than those of the photoexcited aromatic triplets described previously,[76] this rule remains the same.[77]

The spin Hamiltonian parameters of these V(III) complexes, along with the corresponding optical spectroscopic data gathered in previous[33,34,42] and current studies, allow us to gain considerable insight into the electronic properties of the V(III) ion in distorted octahedral coordination environments. In an octahedral crystal field, the ^{3}F and ^{3}P free-ion states of V(III) are split to yield the triplet states shown in Figure 9 (g subscripts are omitted). Addition of a trigonal distortion, as appropriate for $V(acac)_3$, further splits the levels as indicated, with the ground state $^3A_2$ derived from $^3T_1$(F).[33,34,38,42] Despite this apparent simplicity, numerous discrepancies exist in previous assignments of the electronic transitions for $V(acac)_3$, which we will briefly explain. Machin and Murray[34] assigned the shoulder at 18 180 cm^{-1} to the transition $^3T_{1g} \rightarrow {}^3T_{2g}$(F) in O_h symmetry and the

(76) Krzystek, J.; von Schütz, J. U. *Adv. Chem. Phys.* **1993**, *86*, 167−329.
(77) Vongtragool, S.; Gorshunov, B.; Dressel, M.; Krzystek, J.; Eichhorn, D. M.; Telser, J. *Inorg. Chem.* **2003**, *42*, 1788−1790.

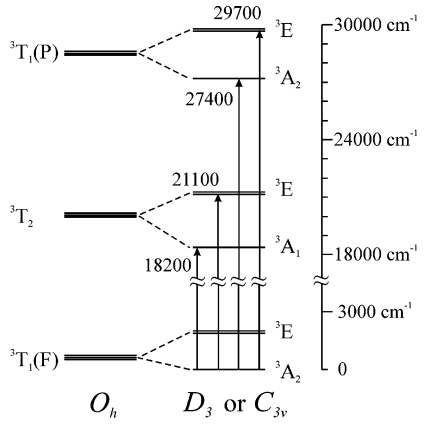

Figure 9. Energy levels of triplet states of V(acac)$_3$ in an octahedral (O_h) ligand field and in a trigonally distorted (D_3 or C_{3v}) ligand field (in C_3 symmetry, the $^3A_1$ and $^3A_2$ states would be simply ^3A). For clarity, the g subscripts have been omitted from the $^3T_{1,2}$ states. The $^3A_2$ state arising directly from ^3F is off-scale. The energy levels are approximately to scale; the energy separation between the ground and excited states is contracted as indicated. The vertical arrows indicate proposed assignments to the LF transitions observed by MCD; the two of these lowest in energy correspond to those observed in the absorption spectrum here and previously.[33,34]

shoulder at 21 740 cm^{-1} to the transition $^3T_{1g} \rightarrow {}^3T_{1g}(P)$. These assignments led them to propose the following parameters: $B = 285$ cm^{-1}; $Dq = 1889$ cm^{-1}.[34] The Dq value is in rough agreement with that originally proposed by Piper and Carlin.[33] This very low value for the Racah interelectronic parameter B (the free-ion value lies in the range of 860−886 cm^{-1})[78,79] is surprising and led Gregson et al. to reanalyze the data and propose instead the following: $B = 600$ cm^{-1}; $Dq = 2225$ cm^{-1}.[42] These newer parameters appear satisfactory, except that they do *not* give electronic transition energies that correspond to the assignments made by Gregson et al.[80] Instead, their transition assignments require $B = 328$ cm^{-1} and $Dq = 1806$ cm^{-1}.[81] Thus the original problem remains, namely that although the value of B is now greater than originally proposed,[34] it is still too low (only ∼40% of the free-ion value).

In an attempt to resolve these discrepancies, we have made use of the MCD results by proposing that both lower-energy LF transitions (at 18 200 and 21 100 cm^{-1}) arise from the parent $^3T_{1g} \rightarrow {}^3T_{2g}$ transition, while LF transitions above 25 000 cm^{-1} are due to the parent $^3T_{1g}(F) \rightarrow {}^3T_{1g}(P)$ transition. As described above, these higher energy LF transitions are unobservable in absorption spectra due to very intense CT and acac ligand $\pi \rightarrow \pi^*$ bands. Possible assignments are as follows: $^3A_2[^3T_{1g}(F)] \rightarrow {}^3A_1(^3T_{2g})$ at 18 200 cm^{-1}; $^3A_2 \rightarrow {}^3E(^3T_{2g})$ at 21 100 cm^{-1}; $^3A_2 \rightarrow {}^3A_2$-$[^3T_{1g}(P)]$ at 27 400 cm^{-1}; $^3A_2 \rightarrow {}^3E[^3T_{1g}(P)]$ at 29 700 cm^{-1}.[82] Use of the full matrix method with these assignments gives an adequate fit (within ∼850 cm^{-1} for transitions to $^3T_2$ and ∼250 cm^{-1} for transitions to $^3T_1(P)$) with $B = 684$ cm^{-1}, $Dq \approx 2000$ cm^{-1}, and a trigonal splitting of ∼2100 cm^{-1}.[83] This trigonal splitting obtained with these assignments is quite large, and consequently, a relatively large spin−orbit coupling constant of $\zeta = 203(3)$ cm^{-1} (essentially the free-ion value)[53,79] is required to match the experimental axial zfs.[84] Another option involves fixing the trigonal splitting in $^3T_1(F)$ to the 1100 cm^{-1} value proposed by Gregson et al.,[42] which requires $Ds = -500$ cm^{-1}. When the two, strong, negative MCD bands at 21 100 cm^{-1} ($^3A_2 \rightarrow {}^3E[^3T_{2g}(F)]$) and 29 700 cm^{-1} ($^3A_2 \rightarrow {}^3E[^3T_{1g}(P)]$) are accounted for, this method gives $B = 647$ cm^{-1} (∼75% of the free-ion value) and $Dq = 2157$ cm^{-1}.[85] Inclusion of spin−orbit coupling, $\zeta = 165$ cm^{-1} (∼80% of the free-ion value) yields $D = +7.44$ cm^{-1}, in good agreement with experiment, although the transition $^3A_2 \rightarrow {}^3A_1[^3T_{2g}(F)]$ is calculated to be ∼2200 cm^{-1} above the observed shoulder at 18 200 cm^{-1}.[86]

We conclude that use of a simple crystal field model to describe the electronic structure of V(III) in V(acac)$_3$ is not entirely satisfactory, although the calculated parameters are not that far from those proposed earlier.[33,34,42] We note that Cr(acac)$_3$ has been the subject of much theoretical and experimental study, and its electronic structure has also proven to be a thorny issue.[87,88] We can only speculate that, in V(acac)$_3$, the possibility of Jahn−Teller effects, such as quantified for *trans*-$[VCl_2(H_2O)_4]^+$,[89] and the properties of the tris acac ligands, whether due to phase coupling (the Orgel effect)[90,91] or "misdirected valency",[87] might lead to an effective trigonal splitting much larger than expected for a homoleptic complex with unidentate ligands. We hope that

(78) Mabbs, F. E.; Collison, D. *Electron Paramagnetic Resonance of d Transition Metal Compounds*; Elsevier: Amsterdam, 1992.

(79) Figgis, B. N.; Hitchman, M. A. *Ligand Field Theory and its Applications*; Wiley-VCH: New York, 2000. See Chapter 3 and references therein for a discussion of the chemical significance of AOM parameters. See p 110 for free-ion Racah and spin−orbit coupling parameters.

(80) The assignments $^3A_2[^3T_{1g}(F)] \rightarrow {}^3E(^3T_{2g})$ at 18 180 cm^{-1} and $^3A_2$-$[^3T_{1g}(F)] \rightarrow {}^3A_2[^3T_{1g}(P)]$ at 21 740 cm^{-1} yield transition energies much higher than observed: 21 830 and 28 940 cm^{-1}, respectively.

(81) This discrepancy is corroborated by full matrix calculations using the trigonal field parameters $B = 347(3)$ cm^{-1}, $Dq = 1810(5)$ cm^{-1}, and $Ds = -450(5)$ cm^{-1}, which give an excellent match of the putative optical transition energies and a trigonal splitting of 1100 cm^{-1}. Inclusion of spin−orbit coupling, $\zeta = 160$ cm^{-1} (equivalent to $\lambda = \zeta/2S = 80$ cm^{-1}; the same as used by Gregson et al.,[42] with $C = 1400$ cm^{-1} ($C \equiv 4B$)) yields an axial zfs in excellent agreement with experiment: $D = +7.43$ cm^{-1}.

(82) In D_3 symmetry, $A_2 \rightarrow E$ transitions are x,y-dipole allowed, $A_2 \rightarrow A_1$ is z-allowed, but the transition $A_2 \rightarrow A_2$ is dipole forbidden, making the assignment to $^3A_2 \rightarrow {}^3A_2[^3T_{1g}(P)]$ the most questionable. However in C_3, $A \rightarrow A$ is z-allowed and the rhombic zfs observed for V(acac)$_3$ suggests that the effective symmetry is low so that dipole allowedness should not be a major factor.

(83) The trigonal splitting even in $[V(H_2O)_6]^{3+}$ (i.e., no chelating ligands) is quite large; as determined by electronic Raman spectroscopy it equals 1940 cm^{-1}.[31]

(84) Calculation of axial g values with eqs 2 and these parameters with $k = 1$ yields $g_\perp = 1.84$ and $g_{||} = 1.94$, in reasonable agreement with the experimental value for g_x. The experimental value for g_z is probably too high, and in any case, the Stevens orbital reduction parameter, k_z ($k_{||}$), could be lowered to bring the calculated g_z to ca. 2.00.

(85) A possible assignment of $^3A_2 \rightarrow {}^3E[^3T_{1g}(P)]$ at 32 600 cm^{-1} requires $Ds = -550$ cm^{-1} and gives $Dq = 2183$ cm^{-1} but with $B = 858$ cm^{-1}—the free-ion value—which is unreasonable.

(86) With $k = 1$, the values $g_\perp = 1.78$ and $g_{||} = 1.94$ are calculated, the former in excellent agreement with the experimental $g_\perp = [(g_x^2 + g_y^2)/2]^{1/2} = 1.78$.

(87) Atanasov, M.; Schönherr, T. *Inorg. Chem.* **1990**, *29*, 4545−4550.

(88) Ribbing, C.; Pierloot, K.; Ceulemans, A. *Inorg. Chem.* **1998**, *37*, 5227−5232.

(89) Bussière, G.; Beaulac, R.; Cardinal-David, B.; Reber, C. *Coord. Chem. Rev.* **2001**, *219*−*221*, 509−543.

(90) Ceulemans, A.; Dendooven, M.; Vanquickenborne, L. G. *Inorg. Chem.* **1985**, *24*, 1153−1158.

(91) Schäffer, C. E.; Yamatera, H. *Inorg. Chem.* **1991**, *30*, 2840−2853.

our experimental study might inspire a similarly deeper analysis of $V(acac)_3$.

We next consider the two V(III)−thf complexes. The molecular structure of $VCl_3(thf)_3$ has meridional geometry and thus approximate C_{2v} symmetry.[27] Chart 1 shows the local structure of $VCl_3(thf)_3$ as determined by Cotton et al.[27] They described the bonding in the series $MCl_3(thf)_3$ (M = Sc, Ti, V, Cr) as having axial and equatorial M−Cl and M−O bonds, where the axial bonds are defined as Cl trans to O and the equatorial bonds are defined as Cl trans to Cl and O trans to O.[92] $VCl_3(thf)_3$ may thus be considered as a tetragonally distorted system rather than trigonally distorted like $V(acac)_3$. No structure has been reported for $VBr_3(thf)_3$, but we will assume the same *mer* geometry as found in the $MCl_3(thf)_3$ series.

Spectroscopic data and analysis for $VCl_3(thf)_3$ were given by Machin and Murray,[34] who reported electronic transitions at 12 900 and 20 120 cm^{-1}, assigned to $^3T_1(F) \rightarrow {}^3T_2$ and $^3T_1(F) \rightarrow {}^3T_1(P)$, respectively. As described above, these values are in good agreement with the better resolved MCD LF bands at 13 500 cm^{-1} and at 19 300 and 20 200 cm^{-1}. The originally reported transitions can be fit with the analytical equations for an octahedral complex using B = 554 cm^{-1} and Dq = 1399 cm^{-1}, while use of the values from MCD requires B = 484 cm^{-1} and Dq = 1451 cm^{-1}. In contrast to the situation described above for $V(acac)_3$, the value for B is not unreasonable, ∼60% of the free-ion value.[78,79] The value for Dq is as expected lower than that for $V(acac)_3$ and $[V(H_2O)_6]^{3+}$,[93] complexes with stronger field ligands.

Further analysis requires directly incorporating the rhombic (C_{2v}) symmetry of $VCl_3(thf)_3$, which is best done using the angular overlap model (AOM).[63] This approach has been used to analyze HFEPR data by us[23,61] and others.[24,25,94] As shown in Chart 1, the C_2 ($Cl_{ax}-V-O_{ax}$) axis is defined as z[27] and the $Cl_{eq}-V-Cl_{eq}$ axis we define arbitrarily as x and the $O_{eq}-V-O_{eq}$ axis as y. In our approximate treatment, we employ idealized meridional geometry about V(III).[95] The chloro ligands are considered to have cylindrical π-bonding ($e_{\pi s(y)} \equiv e_{\pi c(x)}$); however, this is unlikely to be the case for the thf ligands. We will assume, by analogy with the hexaaqua complex,[24,25] that one type of π-bonding for the thf ligands is zero. In the coordinate system for $VCl_3(thf)_3$, $e_{\pi c(x)}$ corresponds to equatorial thf π-bonding that is parallel to the z axis (bonding to $d_{xz,yz}$) but perpendicular to an idealized equatorial thf plane, while $e_{\pi s(y)}$ corresponds to π-bonding perpendicular to this axis (bonding to d_{xy}) but in the thf plane. In the thf frame of reference, we therefore assume that $e_{\pi\perp} \equiv e_{\pi c(x)} \neq 0$ and $e_{\pi\parallel} \equiv e_{\pi s(y)} = 0$. We realize that the equatorial thf ligands are not planar but are oppositely tilted roughly 38° with respect to the $Cl_{eq}-V-Cl_{eq}$ (x) axis; the axial thf ligand is likewise rotated with respect to this axis. A twist angle, ψ, was included for the hexaqua complex[24,25] and should be considered for the thf ligands here.

Concerning the AOM bonding parameters, we use as a starting point the octahedral splitting, $10Dq = 3e_\sigma - 4e_\pi \approx$ 14 000 cm^{-1}, deduced above, combined with parameters determined for related complexes, such as those containing Cr(III),[79,96] V(III),[24,25] and our own work on Ni(II).[23,97] This initial choice of parameters (with B = 500 cm^{-1}) gives a reasonable representation of the electronic structure of $VCl_3(thf)_3$ with a $^3B_1$ ground state with a $^3B_2$ first excited state (the two arising from ^3E in 4-fold symmetry). There are $^3A_1$ and $^3B_2$ states (from $^3T_2(F)$) at ∼13 000−14 000 cm^{-1} above the ground state, and the three states arising from $^3T_1(P)$ are calculated at ∼19 500−21 500 cm^{-1}. Electronic transitions from $^3B_1$ are allowed except to $^3B_2$; however, if the effective symmetry is C_2, then all transitions are allowed. These calculated transition energies are in good agreement with our spectroscopic data.

For corroboration with the spin Hamiltonian parameters, we employ a representative, fit-derived, set of AOM parameters (e_σ(Cl) = 5430, e_π(Cl) = 1110 cm^{-1}; thf parameters as above) with B = 480 and C = 2000 cm^{-1} (∼4.2 B) and with a spin−orbit coupling constant of ζ = 150 cm^{-1}. These parameters yield a negative zfs with a significant rhombic component, $D = -10.3$, $|E| = 1.88$ cm^{-1}, and $|E/D| = 0.18$, in good agreement with the VTVH-MCD results. Excited states with predominantly triplet character are calculated to occur at ∼12 700 cm^{-1} and at ∼13 740 cm^{-1}, which would correspond to the MCD band at 13 500 cm^{-1}; other triplet states are in the range 19 500−20 500 cm^{-1}, corresponding to the bands at 19 300 and 20 200 cm^{-1}. This analysis of the electronic structure of $VCl_3(thf)_3$ is very approximate and by no means a unique solution, but it does accommodate the salient structural and spectroscopic features of this complex.

As described above, the MCD spectra for $VBr_3(thf)_3$ are similar to those of the corresponding chloro complex, except for a general red-shift of the bands, particularly those with CT character. In contrast to $VCl_3(thf)_3$, there is no resolved splitting of the band at 18 500 cm^{-1}; therefore, it is possible only to assign the band at 12 600 cm^{-1} to the transition $^3T_1(F) \rightarrow {}^3T_{2g}(F)$ and that at 18 500 cm^{-1} to $^3T_1(F) \rightarrow {}^3T_{1g}(P)$ in O_h symmetry, which yields B = 457 and Dq = 1356 cm^{-1}.

Structural data are lacking for $VBr_3(thf)_3$; however, we assume that the complex has meridional geometry as does the chloro complex. Analysis of the MCD spectra provides estimates for crystal-field parameters that can then be combined with the results for the chloro complex to yield

(92) In $VCl_3(thf)_3$, the two $V-Cl_{eq}$ bonds are essentially the same length and slightly longer than the $V-Cl_{ax}$ bond (2.330(4) vs 2.297(2) Å) while the two $V-O_{eq}$ bonds are nearly the same length but slightly longer than the $V-O_{ax}$ bond (2.062(8) vs 2.102(3) Å).[27]

(93) Lever, A. B. P. *Inorganic Electronic Spectroscopy*, 2nd ed.; Elsevier: Amsterdam, 1984.

(94) Barra, A.-L.; Gatteschi, D.; Sessoli, R.; Abbati, G. L.; Cornia, A.; Fabretti, A. C.; Uytterhoeven, M. G. *Angew. Chem., Int. Ed. Engl.* **1997**, *36*, 2329−2331.

(95) The $Cl_{ax}-V-O_{ax}$ bond angle is 179.64°, the $Cl_{ax}-V-Cl_{eq}$ bond angles are 92.0(5)°, the $Cl_{ax}-V-O_{eq}$ bond angles are 93.7(1)°, and the $Cl_{eq}-V-O_{eq}$ bond angles are essentially 90°.[27]

(96) Gerloch, M.; Slade, R. C. In *Ligand-Field Parameters*; Cambridge University Press: Cambridge, U.K., 1973.

(97) These studies led us to propose AOM bonding parameters for Cl of $e_\sigma \approx 5500$ cm^{-1} and $e_\pi \approx 1100$ cm^{-1} ($e_{\pi s(y)} \equiv e_{\pi c(x)}$) and for the thf ligands of $e_\sigma \approx 6000$ cm^{-1} and $e_{\pi\perp} \approx 1000$ cm^{-1} ($e_{\pi\parallel} \equiv 0$).

an approximate AOM analysis. We fix the AOM bonding parameters for thf in the Br complex to those used in the treatment of the Cl complex but noting that, for Br in Cr(III) complexes, $e_\sigma \approx 5400$ cm^{-1}, somewhat less than that for Cl,[79] we reduce the Br bonding parameters relative to those for the Cl complex. With these assumptions as a starting point for a fitting procedure to the electronic transitions, the resulting values are $B = 456$ cm^{-1}, as in the crystal-field fit, and $e_\sigma(\mathrm{Br}) = 4940$ cm^{-1} and $e_\pi(\mathrm{Br}) = 1010$ cm^{-1}. These parameters yield a $^3B_1$ ground state with $^3A_1$ and $^3B_2$ excited states at $\sim$12 300$-$12 600 cm^{-1} and $^3B_1$-[$^3T_1$(P)] at $\sim$18 500 cm^{-1} above the ground state (the remaining states from $^3T_1$(P) are obscured by CT bands). Inclusion of spin$-$orbit coupling, $\zeta = 210$ cm^{-1}, with $C = 1900$ cm^{-1} yields $D \approx +16$ cm^{-1}, with $|E/D| \approx 0.26$. The magnitudes are in excellent agreement with experiment, but the positive sign of zfs contradicts the negative value observed experimentally. However, the calculated splitting of the ground state triplet is highly rhombic, so that slight shifts in the energy levels within the ground-state spin$-$orbit triplet could change the sign of the zfs.

A negative sign of zfs can be achieved if a twist angle ($\psi_{\mathrm{thf-ax}}$) for the axial thf ligand is introduced, which is reasonable on the basis of the structure of the Cl complex. As this twist angle is increased from zero, the zfs becomes more rhombic so that, at a value of $\psi_{\mathrm{thf-ax}} \approx 23°$, the maximum rhombicity is achieved ($|E/D| = 1/3$) and further increases in $\psi_{\mathrm{thf-ax}}$ give a negative zfs. At $\psi_{\mathrm{thf-ax}} = 40°$, $|E/D| \approx 0.23$—the same value as observed experimentally. In this case, the magnitude of the zfs is slightly smaller than the experimental value ($D \approx -14$ cm^{-1}), but adjustments in both the angle and spin$-$orbit coupling suggest that the ranges $\psi_{\mathrm{thf-ax}} = 35(5)°$ and $\zeta = 225(5)$ cm^{-1} yield $D \approx -16$ cm^{-1} with $|E/D| \approx 0.23$. Although it appears problematic that the required value for ζ is that ca. 5$-$10% greater than the free-ion value, this might be due to contributions from spin delocalization onto the Br ligands. The value of ζ_{np} for Cl is only 587 cm^{-1}, while that for Br is 2457 cm^{-1}.[98] Thus, qualitatively, any formally Br atom character in the ground-state wave function would lead to an effective increase in ζ_{nd} for vanadium. Note that for $NiI_2(PPh_3)_2$ a large spin$-$orbit coupling constant was needed,[23] and in an iodo complex of Mn(III), Mossin et al. found that a simple $3d^4$ model was not sufficient to explain the zfs, due to the contributions of the iodo ligands.[99]

Additional support for this model comes from the calculation of g values with use of the above ligand-field parameters. When $k = 1$, calculations with eqs 2 yields $g_x = 1.79$, $g_y = 1.77$, and $g_z = 1.60$, and a modest inclusion of orbital reduction, namely $k_{x,y} = 0.8$ and $k_z = 0.7$, yields $g_x = 1.82$, $g_y = 1.78$, and $g_z = 1.72$, in reasonable agreement with the experimental values of $g_x = 1.86(1)$, $g_y = 1.90(1)$, and $g_z = 1.710(4)$. The overall ordering, $2.0 > g_x \approx g_y > g_z$, is predicted by this ligand-field model, and more importantly, the unusually low value observed for g_z is reproduced in the calculation.

Conclusions

High-frequency and -field EPR spectroscopy, in conjunction with optical spectroscopy (absorption, MCD) and magnetic measurements (VTVH-MCD and susceptibility), have been used in concert to probe the non-Kramers, $S = 1$, V(III) ion in two types of pseudooctahedral complexes: $V(acac)_3$ and $VX_3(thf)_3$ (X = Cl, Br). The former has a trigonally distorted geometry, and the latter two have meridional geometries, thus representing two different forms of six-coordinate complexes. All three of these complexes are "EPR silent" at conventional fields and frequencies; however, the use of high fields (up to 25 T) and sub-THz wave energies (up to 23 cm^{-1}, 700 GHz) reveals a large number of magnetic resonance transitions, particularly for $VBr_3(thf)_3$. Analysis of the tunable-frequency HFEPR data for $V(acac)_3$ and $VBr_3(thf)_3$ yields precise sets of spin Hamiltonian parameters for both complexes that are in excellent agreement with those from VTVH-MCD analyses. For $VCl_3(thf)_3$, only one zero-field HFEPR transition is observed; however, VTVH-MCD and magnetic measurements give a reasonable set of spin Hamiltonian parameters. The complexes all exhibit large axial zfs, with D ranging from ca. +8 cm^{-1} in $V(acac)_3$ to ca. -16 cm^{-1} in $VBr_3(thf)_3$. Significant rhombic zfs is also observed, with the limit $|E/D| = 1/3$ approached in the thf complexes. The combination of spin Hamiltonian parameters from HFEPR/VTVH-MCD with optical spectroscopic data from MCD has permitted detailed ligand-field analyses that advance our understanding of the bonding in these complexes. In particular, earlier inconsistencies regarding $V(acac)_3$ have been resolved and novel information on the thf complexes, including estimates of the AOM bonding parameters, have been obtained.

This study thus both provides an example of the utility of the HFEPR technique in the study of integer-spin transition metal complexes and gives detailed information on the electronic structure of a relatively less studied ion, V(III), which can be of use in developing new molecular materials, such as single-molecule magnets. Specifically, the mononuclear building blocks must combine to yield an overall negative zfs for the material to exhibit the magnetic bistability characteristic of single-molecule magnets. Constitutive building blocks with negative zfs are thus a desirable, although not necessarily sufficient, requirement. We show here that $VX_3(thf)_3$ complexes have $D < 0$, unlike, to our knowledge, all hitherto characterized complexes of V(III), such as those with O_6 donor sets. Thus, these halo$-$thf complexes are of potential use in the assembly of high-spin magnetic materials.

Acknowledgment. The NHMFL is funded by the NSF through Cooperative Agreement DMR 0084173 and the State of Florida. Roosevelt University and the NHMFL User Program supported J.T. The Alfred P. Sloan Foundation

(98) Jørgensen, C. K. In *Absorption Spectra and Chemical Bonding in Complexes*; Pergamon Press: Oxford, U.K., 1962; p 159.
(99) Mossin, S.; Weihe, H.; Barra, A.-L. *J. Am. Chem. Soc.* **2002**, *124*, 8764$-$8765.

supported J.J.S., J.R.L., and T.C.B. The NSF Graduate Research Fellowship Program (A.T.F.) and the Camille and Henry Dreyfus Foundation are also thanked (J.J.S. and J.R.L.). We thank Dr. J. Bendix, Ørsted Institute, University of Copenhagen, Copenhagen, Denmark, for the ligand field analysis software and for great help in implementing both it and our own software. We thank P. Bättig and Prof. C. Daul, University of Fribourg, Fribourg, Switzerland, for help in checking the crystal field analysis programs and the reviewers for many helpful comments.

Supporting Information Available: Four figures (S1−S4) showing optical and magnetic spectroscopic data for the three complexes of interest. This material is available free of charge via the Internet at http://pubs.acs.org.

IC0493503